THE JOURNAL OF PHYSICAL CHEMISTRY Letters

Evidence for the Dominance of Carrier-Induced Band Gap Renormalization over Biexciton Formation in Cryogenic Ultrafast Experiments on MoS_2 Monolayers

Ryan E. Wood,[∇] Lawson T. Lloyd,[∇] Fauzia Mujid, Lili Wang, Marco A. Allodi, Hui Gao, Richard Mazuski, Po-Chieh Ting, Saien Xie, Jiwoong Park, and Gregory S. Engel*

Cite This: J. Phys. Chem. Lett. 2020, 11, 2658−2666 Read Online

ACCESS | Metrics & More | Article Recommendations | SI Supporting Information

ABSTRACT: Transition-metal dichalcogenides (TMDs) such as MoS_2 display promising electrical and optical properties in the monolayer limit. Due to strong quantum confinement, TMDs provide an ideal environment for exploring excitonic physics using ultrafast spectroscopy. However, the interplay between collective excitation effects on single excitons such as band gap renormalization/exciton binding energy (BGR/EBE) change and multiexciton effects such biexciton formation remains poorly understood. Using two-dimensional electronic spectroscopy, we observe the dominance of single-exciton BGR/EBE signals over optically induced biexciton formation. We make this determination based on a lack of strong PIA features at $T = 0$ fs in the cryogenic spectra. By means of nodal line slope analysis, we determine that spectral diffusion occurs faster than BGR/EBE change, indicative of distinct processes. These results indicate that at higher sub-Mott limit fluences, collective effects on single excitons dominate biexciton formation.

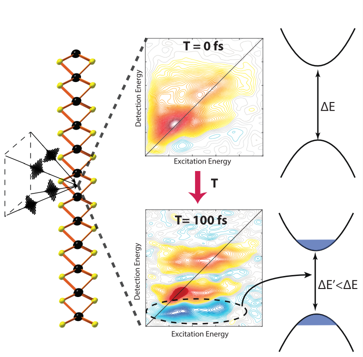

Transition-metal dichalcogenides (TMDs) are semiconducting materials that achieve distinct electronic and optical properties in the monolayer limit. Much like graphene, TMDs can be fabricated as single-layer sheets via mechanical exfoliation or chemical vapor deposition on the wafer scale,[1,2] yielding physical properties distinct from those of the bulk material.[1,3] However, unlike graphene, TMDs are semiconductors and undergo an indirect-to-direct band gap transition in the monolayer limit.[1,3,4] This direct band gap and miniature size allow for the creation of devices with excellent optoelectronic properties, including photodetectors,[5−7] light-emitting diodes,[8,9] solar cells,[10] and transistors.[2,11,12] The extreme quantum confinement achieved in the monolayer limit likely facilitates these exceptional properties via reduced Coulombic screening.[4] Most notably, this reduced screening and confinement can lead to more facile quasiparticle formation[13] as well as nonequivalent valleys in the band structure caused by broken inversion symmetry.[14,15] Exciton formation is heavily favored in TMDs, with exciton binding energies in the range of hundreds of meV.[16−19] The formation of trions,[20−22] biexcitons,[20,23,24] and even higher-lying exciton−trion complexes[25] has also been reported in TMDs. In particular, a number of reports on TMDs have indicated the persistence of biexcitons at room temperature.[26,27] However, the impact of biexcitons on the optoelectronic properties of TMDs relative to other aspects of carrier dynamics remains an open area of investigation, in part due to the overlapping spectroscopic signals produced by band gap renormalization, the exciton binding energy change, and optically induced biexciton formation in ultrafast spectroscopic experiments.

Ultrafast spectroscopy enables the measurement of excited-state dynamics in a variety of systems, from isolated molecules[28] and photosynthetic complexes[29,30] to nanomaterials,[31,32] by using femtosecond laser pulses. Previous studies have used ultrafast pump−probe spectroscopy to investigate exciton−exciton annihilation,[33,34] band gap renormalization,[35,36] and the formation of intervalley biexcitons[23,37] in TMDs. However, spectroscopic signals from higher-lying excitonic complexes such as biexcitons or trions can often be masked by signals from single-exciton processes, including band gap renormalization, exciton binding energy changes, and carrier-induced broadening. These potentially overlapping signals can lead to controversies surrounding the interpretation of spectroscopic data. One particular long-standing controversy involves the bathochromic shift of the photoinduced absorption (PIA) features in TMDs. These features have been ascribed to exciton to biexciton transitions[38−40] or, alternately, to a mixture of the exciton binding energy change

Received: January 16, 2020
Accepted: March 13, 2020
Published: March 13, 2020

https://dx.doi.org/10.1021/acs.jpclett.0c00169
J. Phys. Chem. Lett. 2020, 11, 2658−2666

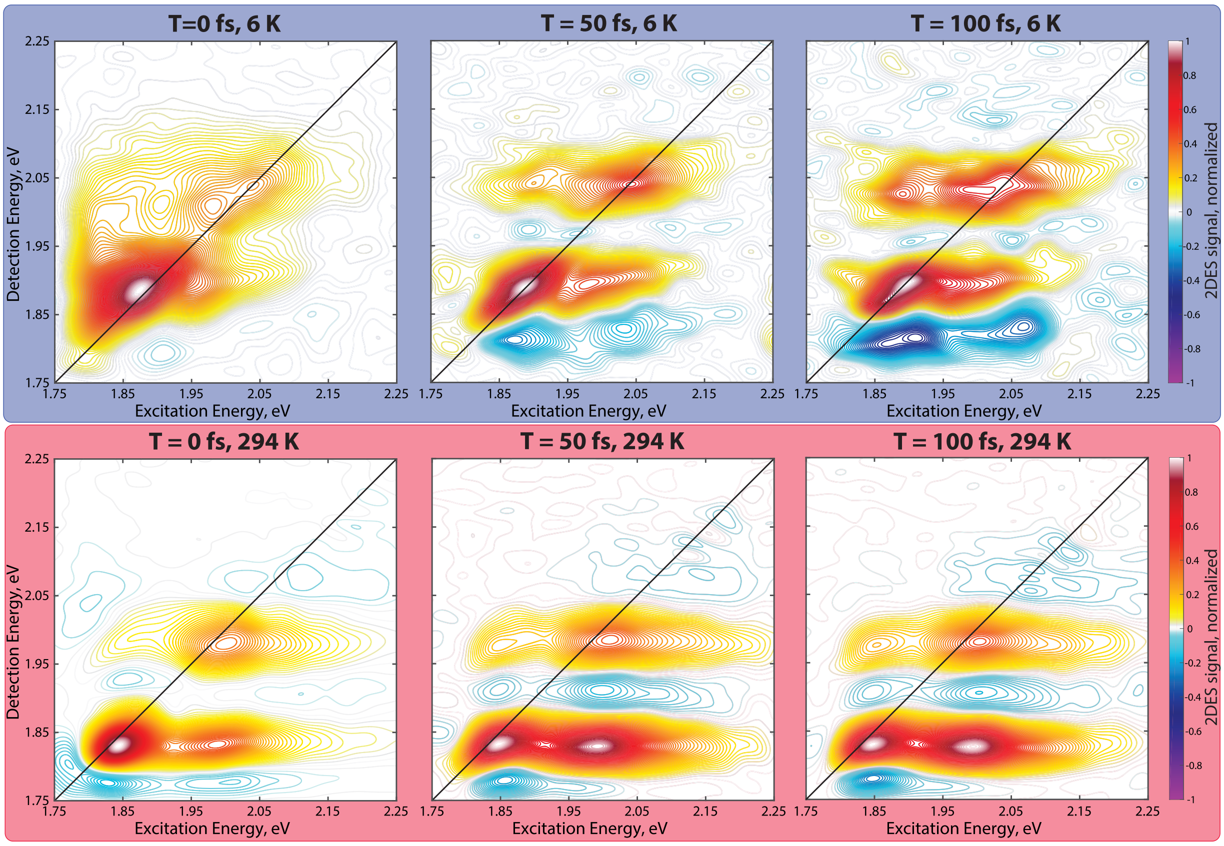

Figure 1. Absorptive real-valued 2DES spectra obtained for CVD-grown monolayer MoS_2 at temperatures of (top row) 6 and (bottom row) 294 K. Cryogenic spectra do not display a strong photoinduced absorption (PIA) feature (E_{ex} = 1.87 eV, E_{det} = 1.81 eV) at T = 0 fs, indicating a lack of optically induced biexciton formation. The growth of a PIA feature as a function of waiting time is indicative of band gap renormalization. At room temperature, the PIA feature (E_{ex} = 1.85 eV, E_{det} = 1.77 eV) is present at T = 0 fs but continues to grow in as a function of waiting time. This feature is still ascribed to band gap renormalization. At all temperatures, a cross peak corresponding to exciting at B and detecting at A (6 K: E_{ex} = 2.015 eV, E_{det} = 1.89 eV) is observed, indicative of excitonic coupling and potential energy transfer from the B to the A exciton. Each frame is separately normalized, and the data is plotted with 100 contours. As signal decays (Figures S9 and S10), the noise becomes more visible in the lowest-amplitude contours at later waiting times. Thus, small features even several contours high at long times likely arise from experimental noise and are not due to the electronic structure of the sample.

and carrier-induced band gap renormalization (BGR/EBE).[36,41]

Biexciton formation is subject to a selection rule forcing the biexciton to occur in the valley opposite to that from initial excitation, while band gap renormalization is thought to occur mainly in the same valley as excitation.[23] As such, previous reports have assigned the observed PIA feature to an intervalley exciton-to-biexciton transition by leveraging a comparison between a cross-circularly polarized sequence and a cocircularly polarized sequence at cryogenic temperature.[23,37] By contrast, other reports have assigned the PIA features to the BGR/EBE change by using cross-linearly polarized pulses and theoretical calculations in room-temperature experiments.[36] Moreover, co- or cross-circularly polarized excitation is not entirely germane to the operating conditions of most optoelectronic devices, which absorb unpolarized or linearly polarized light under typical operating conditions. To resolve this PIA assignment controversy and ascertain the relative strengths of these competing biexciton formation and BGR/EBE effects, an experimental study capable of seeing both effects without preference and unambiguously assigning the PIA feature is needed. Pump−probe spectroscopy cannot distinguish between these features because there is no way to correlate excitation energy with detection energy while preserving the femtosecond time resolution.

In this work, we use two-dimensional electronic spectroscopy (2DES) to probe the femtosecond dynamics of MoS_2 monolayers at both room temperature and 6 K. 2DES enables the excitation frequency to resolve ultrafast measurements on the 10 fs time scale.[42−44] This time resolution allows us to distinguish competing physical processes on the 10−100 fs time scale that are not resolvable in pump−probe measurements. Optically induced biexciton formation should be achievable instantaneously, while the BGR/EBE change should be delayed relative to excitation on a sub-100-fs characteristic time scale.[45] By coupling the time resolution with the two-dimensional correlation map created by 2DES, we clearly show that BGR/EBE change dominates any optically induced biexcitonic effects in the sub-Mott high-carrier limit. We also uncover a difference in the time scale between the spectral diffusion of exciton signals and the BGR/EBE change in MoS_2 monolayers, indicating possible differing mechanisms for the frequency−frequency correlation function decay and BGR/EBE change.

MoS_2, the first TMD isolated in the monolayer limit, is the most widely characterized TMD and has been studied in the majority of ultrafast reports of band gap renormalization[36,46]

https://dx.doi.org/10.1021/acs.jpclett.0c00169
J. Phys. Chem. Lett. 2020, 11, 2658−2666

and biexciton effects.[24,27,37,38] A previous 2DES study used the simultaneous ultrafast time and excitation frequency resolution to document an exchange-driven mixing of the A and B excitonic transitions in MoS_2. However, this study did not distinguish between negative and positive signals and thus lacked the ability to distinguish PIA from stimulated emission (SE) and ground-state bleach (GSB) signals.[47] Here, we use 2DES in an attempt to distinguish between the BGR/EBE change and optically induced biexciton formation explanations for the below band gap PIA detailed in the MoS_2 literature. 2DES spectra on wafer-scale CVD-grown MoS_2 are recorded in transmission geometry using an all-reflective delay setup described in detail previously[48] and are phased to independently acquired pump−probe measurements using the projection-slice theorem.[49] All four of the beams used in this experiment are colinearly polarized, enabling us to observe dynamics in both valleys in MoS_2 and compare the relative strengths of optically induced biexciton formation and BGR/EBE change. This colinearly polarized study more closely resembles the operating conditions of optoelectronic devices such as photodetectors or solar cells. Cryogenic temperatures and higher sub-Mott limit fluences of 16 μJ/cm^2 per beam for both cryogenic and room-temperature experiments were chosen to promote biexciton formation, consistent with other reports in the literature[37,50,51] and the expected power-law dependence of band gap renormalization.[52] We calculate the total carrier density of both A and B excitons induced by our broadband laser pulse to be 4×10^{12} carriers per cm^2 for room-temperature experiments. We note that this carrier density calculation most likely leads to an overestimate of the carrier concentration since it is difficult to remove reflection and scattering terms from the steady-state absorption spectrum used to calculate the percentage of incident photons absorbed. While we are unable to calculate an exact carrier density for the cryogenic experiments, we expect that it will be similar due to the broadband nature of our laser pulse. These carrier densities are similar to other ultrafast studies of BGR/EBE change in TMDs[35,36,53] and lie in the third-order regime as demonstrated by Guo et al.[47]

2DES data showing the excitonic dynamics in MoS_2 at both cryogenic and room temperature for representative waiting times are shown in Figure 1. At both temperatures, we observe positive features along the diagonal, corresponding to ground-state bleaches from the A (6 K: E_{ex} = 1.89 eV, E_{det} = 1.89 eV) and B (6 K: E_{ex} = 2.04 eV, E_{det} = 2.04 eV) excitons. We also observe positive cross-peaks both above and below the diagonal, corresponding to coupling between the A and B excitonic states (6 K: E_{ex} = 1.89 eV, E_{det} = 2.042 eV) as well as potential energy transfer from the B to the A exciton (6 K: E_{ex} = 2.015 eV, E_{det} = 1.89 eV). The appearance of the above-diagonal coupling cross peak, for which a number of mechanisms have been proposed, has been well documented previously in 2DES[47] and pump−probe experiments.[54−56] Coupling between the A and B excitonic states in monolayer TMDs has been previously ascribed to an exchange-driven mixing,[47] a spin-flip in the pumped valley,[57,58] exciton−exciton scattering,[59] Dexter-like intervalley coupling of the A and B excitonic transitions,[54,60] or a joint action of exchange coupling and phonon-mediated thermalization into dark excitons.[55] We are unable to distinguish between any of these proposed mechanisms due to the linear polarization used in these experiments, which precludes obtaining valley-specific information. These positive features are observed at all time points, with decay corresponding to exciton−exciton annihilation of the A-exciton, potential transfer from the B to A exciton, and other decay pathways. Features in the 2DES spectra, especially at cryogenic temperatures, are substantially broader than what would be expected from the linear absorption spectra seen in the literature.[61] While extensive analysis of this broadening is beyond the scope of this work, potential mechanisms include excitation-induced dephasing[47,62] and carrier-induced broadening,[63] which have previously been observed in spectra of TMDs. Given the appearance of this broadening at early waiting times, including T = 0, EID is the most likely mechanism responsible.[64,65] We are unable to comment further in this letter due to a lack of fluence-dependent 2DES data, which could potentially provide experimental evidence for the mechanisms of the broad line shapes observed in this work.[62] We note that spectral features in the 2DES spectrum are elongated along the excitation axis, particularly in the room-temperature spectra. This elongation has been previously observed in multidimensional spectra of four-layer MoS_2[66] as well as in 2DES spectra of quantum well systems,[67−72] particularly when using a colinear polarization sequence.[71] This elongation has been ascribed to many-body effects, including exciton−exciton interactions,[70,73,74] exciton-free carrier scattering,[67] and excitation-induced dephasing.[68] Due to the presence of many excitons and potentially free carriers, it is highly likely that similar mechanisms are responsible for the broadening observed in the 2DES spectra in Figure 1. Further studies including simulation will be necessary to fully uncover the nature of this broadening. Additionally, we observe several negative PIA features in the 2DES map (6 K: E_{ex} = 1.87 eV, E_{det} = 1.81 eV), corresponding to the photoinduced absorption features previously observed in pump−probe spectra.[36,37] The negative features grow in with a time constant characteristic of the BGR/EBE change process. The decay of these features mirrors the decay of the positive features, suggesting that they also report on the population of the excited state.

To determine if the negative 2DES signals in the TMD spectra arise from biexcitons or BGR/EBE change, we look at the 2DES spectra on the sub-100-fs time scale, before BGR/EBE change can occur (Figure 1). We do not observe any signals indicative of excited-state absorption from the single exciton manifold to the biexciton manifold at either cryogenic or room temperature. The cryogenic spectra at T = 0 fs (Figure 1) do not show any appreciable negative features that correspond to PIA. The absence of PIA features cannot conclusively rule out biexciton formation; however, this result does indicate that any potential signature of optically induced biexciton formation is not visible over the positive features of the spectrum. It is worth noting that an optically induced biexciton formation process thought to result in a PIA feature in ultrafast spectra is distinct from the spontaneous formation of biexcitons observed in steady-state photoluminescence experiments. The spontaneous process is contingent on two excitons coming together via exciton diffusion, while the optically induced process uses light to produce the second excitation and is not dependent on diffusion. We observe many second-order processes in this sample, which have been previously assigned to exciton−exciton annihilation[34] but also match the expected kinetics of spontaneous biexciton formation.

Spectral signatures corresponding to a spontaneously formed biexciton or higher-order exciton complex would most likely

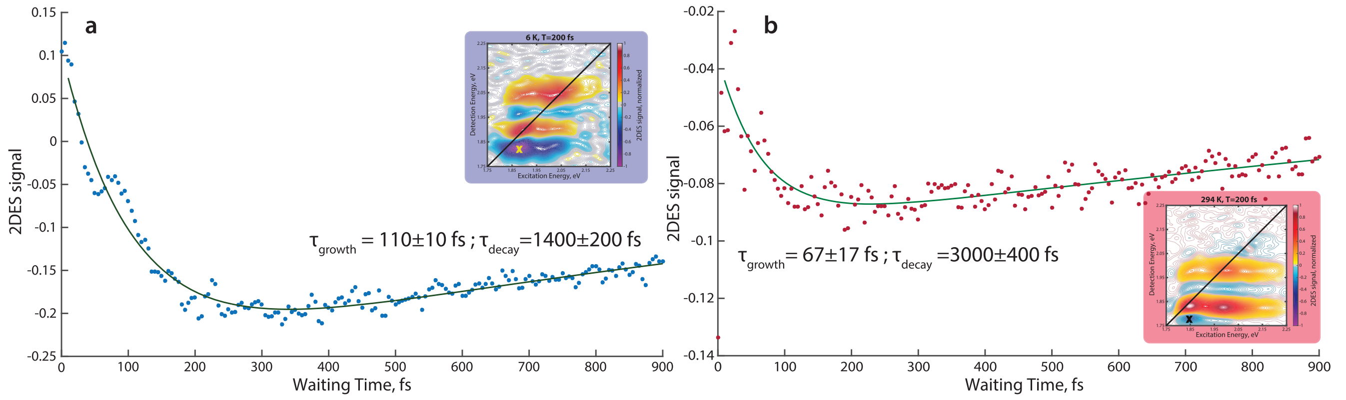

Figure 2. 2DES signal as a function of waiting time corresponding to excitation at the A exciton and detection at the band gap-renormalized A exciton at both (a) cryogenic temperature and (b) room temperature. The point on the spectrum corresponding to the time trace displayed is marked with an X on the inset spectrum. These traces have each been fit to a biexponential function (shown in green), with the first time constant corresponding to the growth of the PIA feature and the second corresponding to its decay. The time dynamics of these traces are characteristic of BGR/EBE change. We observe a faster BGR/EBE change at room temperature, indicative of a phonon-assisted mechanism.

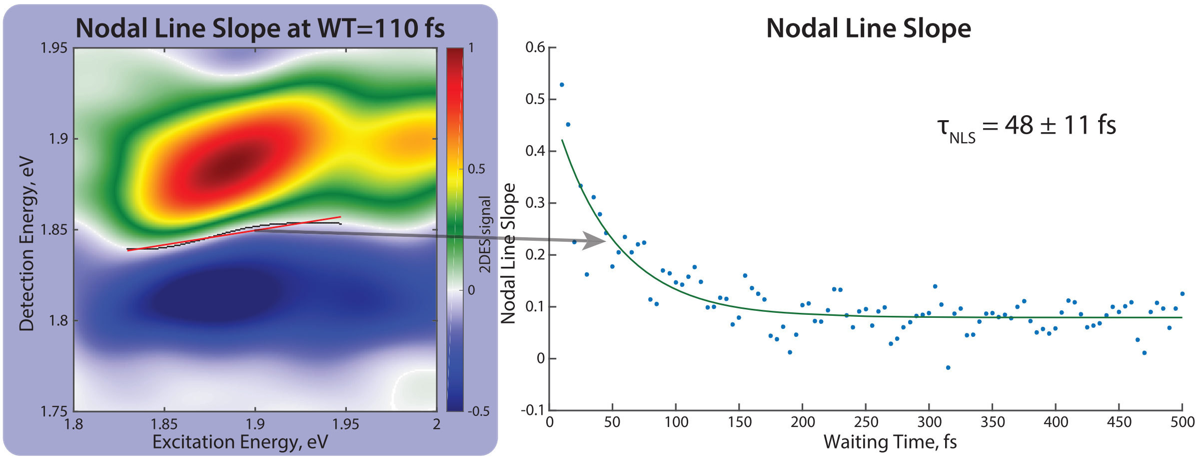

Figure 3. Cryogenic nodal line slope and nodal line slope as a function of waiting time for the A diagonal and band gap-renormalized A node. Nodal line slope relaxation is a measure of the decay of the frequency−frequency correlation function and spectral diffusion. We observe cryogenic nodal line slope relaxation with a decay constant distinct from that of band gap renormalization (shown in Figure 2), indicative of a potential two-step process for band gap renormalization.

take the form of stimulated emission from this state or excited-state absorption to a higher-lying tri- or quadexciton state. We do not observe any stimulated emission signals from potential spontaneously formed biexcitons (in agreement with our observed lack of absorptive transitions to the biexciton state), though these signals may be present and masked by the PIA feature from the BGR/EBE change appearing at the same spectral location. ESA features would most likely be seen at red-shifted energies, potentially outside of the laser bandwidth used in this experiment. As such, we are unable to report on any spontaneous biexciton formation processes. At cryogenic temperature, the PIA features grow in at later waiting times, as seen in Figure 1B,C. At room temperature, PIA signals are indeed present at $T = 0$ fs (Figure 1D). We ascribe these signals to the beginnings of BGR/EBE change, as the signals continue to grow in as a function of waiting time (Figure 1E,F). To find the time scale of BGR/EBE change at cryogenic and room temperatures, we fit the time traces for a given excitation and detection frequency to biexponential functions. Time traces corresponding to the BGR/EBE change dynamics at both room and cryogenic temperatures are shown in Figure 2. From these traces, we extract a characteristic time constant of 110 ± 10 fs for cryogenic temperature and 67 ± 17 fs for room temperature. The accelerated dynamics of the BGR/EBE change at warmer temperatures indicates that carrier relaxation and band-filling proceed faster when they can be assisted by phonons. Our results indicate that single-exciton processes, such as BGR/EBE change, dominate biexciton formation in the high-excitation density regime.

The frequency−frequency correlation function (FFCF), as measured by the nodal line slope (NLS) or center line slope (CLS), should serve as an indicator of how much "memory" the system has of its excitation frequency.[75−77] It is anticipated that the FFCF will decay on a similar time scale to BGR or EBE change since the NLS should not evolve further after the BGR/EBE change as the system will have very little memory of its excitation. Of course, the FFCF may decay faster if spectral diffusion occurs prior to BGR or EBE change. To compare the time scales of decay of the FFCF and BGR/EBE change process, we compare the A-exciton diagonal NLS decay time constants to the BGR/EBE change time constants (from Figure 2) for both cryogenic temperature and room temperature. The NLS at cryogenic temperature is shown in Figure 3, while CLS and NLS analyses for both room temperature and

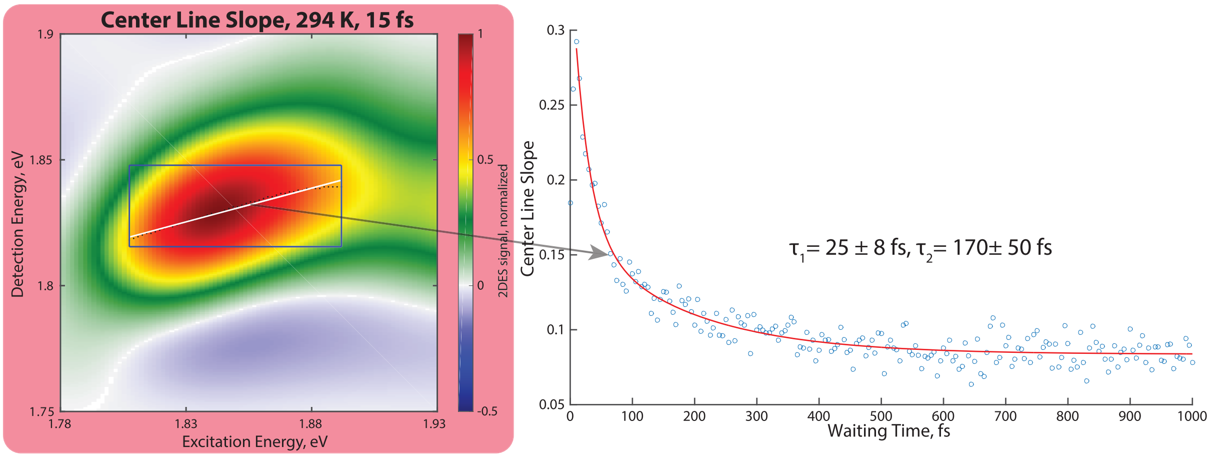

Figure 4. Center line slope analysis for the A-exciton/BGR node at room temperature as a function of waiting time. The biexponential decay of the CLS at room temperature as compared to the monoexponential decay observed at cold temperature indicates that a new pathway for spectral diffusion becomes avaliable at room temperature.

cryogenic temperature are shown in Figures S7−S9 (available in the Supporting Information). NLS relaxation at cold temperatures proceeds with a 48 ± 11 fs time constant. Distinct from the single-exponential decay observed at cryogenic temperature, the NLS and CLS at room temperature follow a biexponential decay (Figures 4 and S7). Such a biexponential decay process is indicative of two different subpopulations, each contributing different dynamics to the overall FFCF decay and corresponding memory loss of the system.[78,79] The CLS analysis for room temperature produces time constants of 25 ± 8 and 170 ± 50 fs (Figure 4). The appearance of a biexponential decay for the FFCF at room temperature is indicative of a new spectral diffusion process that becomes available at higher temperatures. Similar to the BGR/EGE change process, the time scale of the fast component of FFCF decay becomes even faster at room temperature compared to cryogenic temperature, indicative of a phonon-assisted process. Both the PIA feature and the NLS are thought to correspond to carrier relaxation and band filling and as such should have matching time constants. However, a comparison of the NLS and BGR/EBE change time constants for both cryogenic temperature (48 ± 11 vs 110 ± 10 fs) and room temperature (of 25 ± 8 and 170 ± 50 vs 67 ± 17 fs) reveals a substantial discrepancy between the two time constants. This discrepancy is indicative of two different processes for spectral diffusion and BGR/EBE change, as opposed to direct coupling of these processes, even though both processes result from exciton−phonon coupling.

Our results suggest that the BGR/EBE change process dominates optically induced biexciton formation in monolayer MoS_2, even at low temperatures. A lack of edge states in the CVD-grown sample could explain the absence of biexcitions.[80] However, SEM images for this sample available in the Supporting Information (Figure S4) indicate that many grain boundaries exist on the 1 μm scale, which may be able to serve as sites for biexciton formation. We lack the ability to tune the doping density in the sample during the experiment, which has been shown to highly promote biexciton formation.[81,82] Photocarrier-induced BGR/EBE change has been extensively studied in 2D epitaxially grown semiconductor quantum wells, with extensive theoretical and experimental evidence that the energy renormalization of the band gap is proportional to the cube root of the number of carriers.[52,83] However, the kinetics of this process has not been studied previously, and as such we cannot compare our kinetic results to theoretical predictions for 2D systems.[52,83]

In summary, we have used 2DES to demonstrate that BGR/EBE change dominates biexcitonic excited-state absorption signals at both room temperature and cryogenic temperature in MoS_2. We make this assignment based on the absence of the strong negative features in the spectrum at T = 0 fs at cryogenic temperature. BGR/EBE change proceeds faster at room temperature, with a 67 fs time constant at room temperature as compared to 110 fs at 6 K. This behavior is consistent with previous reports of BGR/EBE change[53] as well as documented strong exciton−phonon coupling in MoS_2.[84,85] By comparing the NLS time constant to the BGR/EBE change time constant, we determined that the processes of spectral diffusion and BGR/EBE change are dissimilar and either distinct or a coupled two-step process. Two-dimensional electronic spectroscopy has uncovered this discrepancy by enabling separate direct measurement of the system-bath-carrier relaxation dynamics and BGR/EBE change. The results outlined here should be broadly applicable to other TMDs, such as $MoSe_2$, WSe_2, and WS_2. These TMDs have steady-state photonic properties and band structures similar to those of MoS_2,[3,86] although tungsten-based materials have a different spin-split bright/dark band structure.[87] Previous studies of the BGR/EBE change in MoS_2[36] and WS_2[35] have uncovered similar processes for the BGR/EBE change in these two materials. It is thus likely that the BGR/EBE change will dominate biexciton formation in other TMDs under similar experimental conditions.

Ultrafast Spectroscopic Methods. The 2DES apparatus used in this experiment has been described in detail previously.[48] Briefly, a Ti:sapphire oscillator seeds a Ti:sapphire regenerative amplifier (Coherent Inc., Legend Elite USP), generating a 5 kHz pulse train at a 800 nm center wavelength and a 38 fs pulse width. These pulses are then focused into a 2-m-long tube of argon gas, where they then undergo self-phase modulation to produce a continuum from 500 to 900 nm. This continuum is truncated with a dielectric short-pass filter at 700 nm, rejecting all photon energies substantially below the band gap of MoS_2. The pulse is then compressed to its time-bandwidth product limit with a pulse shaper (MIIPS, Biophotonics Inc.), resulting in a 9 fs pulse that is directed into the 2DES spectrometer. In the 2DES spectrometer, the initial beam is split into four separate beams, and the waiting time (T) and coherence time (τ) delays are encoded by motorized delay stages (Aerotech Inc.). The fourth beam (local oscillator) is attenuated by a factor of 10^5 and used for heterodyne detection. For cryogenic experiments, the sample is cooled in a custom-designed exchange-gas helium flow cryostat (RC-151, Cryo Industries of America) to 6 K. The signal and the heterodyne beam are directed into a commercially available spectrograph and camera (Andor Inc.). The data are processed according to techniques developed previously to balance noise and scatter suppression with line shape preservation[43,88] and are windowed with Hann, Welch, and Tukey windows with minimum side lobes of at least −18 dB. The spectra are phased to independently acquired pump−probe measurements[43,49] and are plotted with 100 contours, chosen to dedicate approximately 1 to 2 contours to the noise in the 2DES spectra.

Sample Growth and Characterization. Monolayer MoS_2 films were grown on fused SiO_2 wafers (University Wafer, Inc.) using metal−organic chemical vapor deposition in a home-built, hot-walled, horizontal tube furnace using a method described in detail previously.[2] SEM measurements were carried out using a Zeiss Merlin field-emission scanning electron microscope with secondary-electron imaging at accelerating voltages of between 1 and 3 kV. Absorption spectra were taken in transmission geometry on a Cary 5000 UV/vis/NIR spectrophotometer. Raman and PL spectra were acquired on a Horiba LabRamHR Evolution confocal Raman microscope using 532 nm excitation.

■ ASSOCIATED CONTENT

Supporting Information

The Supporting Information is available free of charge at https://pubs.acs.org/doi/10.1021/acs.jpclett.0c00169.

> Raman, photoluminescence, and absorption spectra and SEM images of the sample used; the laser spectrum used in the 2DES experiments; 2DES spectra for cryogenic temperature and room temperature to 900 fs; CLS analyses for both cryogenic temperatures; NLS analysis for room temperature; a description of the methods used for the CLS and NLS analyses; time traces corresponding to the B-diagonal peak for both cryogenic temperature and room temperature; a fit of 1-over the A-diagonal time trace for cryogenic and room temperature; the dynamics of the AB above the diagonal cross peak and the BA below the diagonal cross peak; a discussion of the potential contributions to the cross peaks observed in the 2DES spectra; an explanation detailing how the carrier concentration is calculated; and fiduciary data showing 2DES spectra with coherence time and rephasing time window sizes doubled (PDF)

■ AUTHOR INFORMATION

Corresponding Author

Gregory S. Engel − *Department of Chemistry, James Franck Institute, and Institute for Biophysical Dynamics, University of Chicago, Chicago, Illinois 60637, United States;* orcid.org/0000-0002-6740-5243

Authors

Ryan E. Wood − *Department of Chemistry, James Franck Institute, and Institute for Biophysical Dynamics, University of Chicago, Chicago, Illinois 60637, United States*

Lawson T. Lloyd − *Department of Chemistry, James Franck Institute, and Institute for Biophysical Dynamics, University of Chicago, Chicago, Illinois 60637, United States*

Fauzia Mujid − *Department of Chemistry and James Franck Institute, University of Chicago, Chicago, Illinois 60637, United States*

Lili Wang − *Department of Chemistry and James Franck Institute, University of Chicago, Chicago, Illinois 60637, United States;* orcid.org/0000-0002-6298-0302

Marco A. Allodi − *Department of Chemistry, James Franck Institute, and Institute for Biophysical Dynamics, University of Chicago, Chicago, Illinois 60637, United States;* orcid.org/0000-0002-3289-1659

Hui Gao − *Department of Chemistry, James Franck Institute, and Pritzker School of Molecular Engineering, University of Chicago, Chicago, Illinois 60637, United States; Department of Chemistry and Chemical Biology, Cornell University, Ithaca, New York 14853, United States*

Richard Mazuski − *Department of Chemistry, James Franck Institute, and Institute for Biophysical Dynamics, University of Chicago, Chicago, Illinois 60637, United States*

Po-Chieh Ting − *Department of Chemistry, James Franck Institute, and Institute for Biophysical Dynamics, University of Chicago, Chicago, Illinois 60637, United States*

Saien Xie − *Department of Chemistry and James Franck Institute, University of Chicago, Chicago, Illinois 60637, United States; Kavli Institute at Cornell for Nanoscale Science, Cornell University, Ithaca, New York 14853, United States*

Jiwoong Park − *Department of Chemistry, James Franck Institute, and Pritzker School of Molecular Engineering, University of Chicago, Chicago, Illinois 60637, United States*

Complete contact information is available at: https://pubs.acs.org/10.1021/acs.jpclett.0c00169

Author Contributions

$^\nabla$These authors contributed equally to this work.

Notes

The authors declare no competing financial interest.

■ ACKNOWLEDGMENTS

This work was supported by the Vannevar Bush Faculty Fellowship Program (Grant nos. N00014-16-1-2513 and N00014-15-1-0048), the Air Force Office of Scientific Research (AFOSR) (FA9550-18-1-0099 and FA9550-16-1-0347), and the NSF (under grant no. 1900359). This work was also supported by the NSF MRSEC grant programs at the University of Chicago (DMR-1420709) and the Cornell Center for Materials Research (DMR-1719875). R.E.W. acknowledges support from the National Defense Science & Engineering Graduate Fellowship (NDSEG) Program, 32 CFR 168a, funded through the AFOSR and the Department of Defense. F.M. and R.M. acknowledge support from the NSF-GRFP program under grant no. DGE-1746045. M.A.A. acknowledges support from a Yen Postdoctoral Fellowship from the Institute for Biophysical Dynamics at The University of Chicago and from an Arnold O. Beckman Postdoctoral Fellowship from the Arnold and Mabel Beckman Foundation. The authors acknowledge Prof. William Tisdale for useful discussions and thank Dr. Karen M. Watters for scientific editing.

■ REFERENCES

(1) Mak, K. F.; Lee, C.; Hone, J.; Shan, J.; Heinz, T. F. Atomically thin MoS_2: a new direct-gap semiconductor. *Phys. Rev. Lett.* **2010**, *105* (13), 136805.

(2) Kang, K.; Xie, S.; Huang, L.; Han, Y.; Huang, P. Y.; Mak, K. F.; Kim, C.-J.; Muller, D.; Park, J. High-mobility three-atom-thick semiconducting films with wafer-scale homogeneity. *Nature* **2015**, *520* (7549), 656−660.

(3) Splendiani, A.; Sun, L.; Zhang, Y.; Li, T.; Kim, J.; Chim, C.-Y.; Galli, G.; Wang, F. Emerging Photoluminescence in Monolayer MoS_2. *Nano Lett.* **2010**, *10* (4), 1271−1275.

(4) Kuc, A.; Zibouche, N.; Heine, T. Influence of quantum confinement on the electronic structure of the transition metal sulfide TS_2. *Phys. Rev. B: Condens. Matter Mater. Phys.* **2011**, *83* (24), 245213.

(5) Lopez-Sanchez, O.; Lembke, D.; Kayci, M.; Radenovic, A.; Kis, A. Ultrasensitive photodetectors based on monolayer MoS_2. *Nat. Nanotechnol.* **2013**, *8* (7), 497−501.

(6) Gant, P.; Huang, P.; Pérez de Lara, D.; Guo, D.; Frisenda, R.; Castellanos-Gomez, A. A strain tunable single-layer MoS_2 photodetector. *Mater. Today* **2019**, *27*, 8−13.

(7) Wu, G.; Wang, X.; Chen, Y.; Wang, Z.; Shen, H.; Lin, T.; Hu, W.; Wang, J.; Zhang, S.; Meng, X.; Chu, J. Ultrahigh photoresponsivity MoS_2 photodetector with tunable photocurrent generation mechanism. *Nanotechnology* **2018**, *29* (48), 485204.

(8) Ross, J. S.; Klement, P.; Jones, A. M.; Ghimire, N. J.; Yan, J.; Mandrus, D. G.; Taniguchi, T.; Watanabe, K.; Kitamura, K.; Yao, W.; Cobden, D. H.; Xu, X. Electrically tunable excitonic light-emitting diodes based on monolayer WSe_2 p−n junctions. *Nat. Nanotechnol.* **2014**, *9* (4), 268−272.

(9) Withers, F.; Del Pozo-Zamudio, O.; Mishchenko, A.; Rooney, A. P.; Gholinia, A.; Watanabe, K.; Taniguchi, T.; Haigh, S. J.; Geim, A. K.; Tartakovskii, A. I.; Novoselov, K. S. Light-emitting diodes by band-structure engineering in van der Waals heterostructures. *Nat. Mater.* **2015**, *14* (3), 301−306.

(10) Tsai, M.-l.; Su, S.-H.; Chang, J.-K.; Tsai, D.-S.; Chen, C.-H.; Wu, C.-I.; Li, L.; Chen, L.-J.; He, J.-H. Monolayer MoS_2 Heterojunction Solar Cells. *ACS Nano* **2014**, *8*, 8317−22.

(11) Desai, S. B.; Madhvapathy, S. R.; Sachid, A. B.; Llinas, J. P.; Wang, Q.; Ahn, G. H.; Pitner, G.; Kim, M. J.; Bokor, J.; Hu, C.; Wong, H. S. P.; Javey, A. MoS_2 transistors with 1-nanometer gate lengths. *Science* **2016**, *354* (6308), 99.

(12) Radisavljevic, B.; Radenovic, A.; Brivio, J.; Giacometti, V.; Kis, A. Single-layer MoS_2 transistors. *Nat. Nanotechnol.* **2011**, *6* (3), 147−150.

(13) Lin, Y.; Ling, X.; Yu, L.; Huang, S.; Hsu, A. L.; Lee, Y.-H.; Kong, J.; Dresselhaus, M. S.; Palacios, T. Dielectric Screening of Excitons and Trions in Single-Layer MoS_2. *Nano Lett.* **2014**, *14* (10), 5569−5576.

(14) Mak, K. F.; He, K.; Shan, J.; Heinz, T. F. Control of valley polarization in monolayer MoS_2 by optical helicity. *Nat. Nanotechnol.* **2012**, *7* (8), 494−498.

(15) Zeng, H.; Dai, J.; Yao, W.; Xiao, D.; Cui, X. Valley polarization in MoS_2 monolayers by optical pumping. *Nat. Nanotechnol.* **2012**, *7* (8), 490−493.

(16) Ugeda, M. M.; Bradley, A. J.; Shi, S. F.; da Jornada, F. H.; Zhang, Y.; Qiu, D. Y.; Ruan, W.; Mo, S. K.; Hussain, Z.; Shen, Z. X.; Wang, F.; Louie, S. G.; Crommie, M. F. Giant bandgap renormalization and excitonic effects in a monolayer transition metal dichalcogenide semiconductor. *Nat. Mater.* **2014**, *13* (12), 1091−5.

(17) Zhu, B.; Chen, X.; Cui, X. Exciton Binding Energy of Monolayer WS_2. *Sci. Rep.* **2015**, *5* (1), 9218.

(18) Chernikov, A.; Berkelbach, T. C.; Hill, H. M.; Rigosi, A.; Li, Y.; Aslan, O. B.; Reichman, D. R.; Hybertsen, M. S.; Heinz, T. F. Exciton binding energy and nonhydrogenic Rydberg series in monolayer WS_2. *Phys. Rev. Lett.* **2014**, *113* (7), 076802.

(19) Park, S.; Mutz, N.; Schultz, T.; Blumstengel, S.; Han, A.; Aljarb, A.; Li, L.-J.; List-Kratochvil, E. J. W.; Amsalem, P.; Koch, N. Direct determination of monolayer MoS_2 and WSe_2 exciton binding energies on insulating and metallic substrates. *2D Mater.* **2018**, *5* (2), 025003.

(20) Plechinger, G.; Nagler, P.; Kraus, J.; Paradiso, N.; Strunk, C.; Schüller, C.; Korn, T. Identification of excitons, trions and biexcitons in single-layer WS_2. *Phys. Status Solidi RRL* **2015**, *9* (8), 457−461.

(21) Singh, A.; Moody, G.; Tran, K.; Scott, M. E.; Overbeck, V.; Berghäuser, G.; Schaibley, J.; Seifert, E. J.; Pleskot, D.; Gabor, N. M.; Yan, J.; Mandrus, D. G.; Richter, M.; Malic, E.; Xu, X.; Li, X. Trion formation dynamics in monolayer transition metal dichalcogenides. *Phys. Rev. B: Condens. Matter Mater. Phys.* **2016**, *93*(4), DOI: 10.1103/PhysRevB.93.041401.

(22) Mak, K. F.; He, K.; Lee, C.; Lee, G. H.; Hone, J.; Heinz, T. F.; Shan, J. Tightly bound trions in monolayer MoS_2. *Nat. Mater.* **2013**, *12* (3), 207−211.

(23) Steinhoff, A.; Florian, M.; Singh, A.; Tran, K.; Kolarczik, M.; Helmrich, S.; Achtstein, A. W.; Woggon, U.; Owschimikow, N.; Jahnke, F.; Li, X. Biexciton fine structure in monolayer transition metal dichalcogenides. *Nat. Phys.* **2018**, *14* (12), 1199−1204.

(24) Pandey, J.; Soni, A. Unraveling biexciton and excitonic excited states from defect bound states in monolayer MoS_2. *Appl. Surf. Sci.* **2019**, *463*, 52−57.

(25) Hao, K.; Xu, L.; Nagler, P.; Singh, A.; Tran, K.; Dass, C. K.; Schüller, C.; Korn, T.; Li, X.; Moody, G. Coherent and Incoherent Coupling Dynamics between Neutral and Charged Excitons in Monolayer $MoSe_2$. *Nano Lett.* **2016**, *16* (8), 5109−5133.

(26) Paradisanos, I.; Germanis, S.; Pelekanos, N. T.; Fotakis, C.; Kymakis, E.; Kioseoglou, G.; Stratakis, E. Room temperature observation of biexcitons in exfoliated WS_2 monolayers. *Appl. Phys. Lett.* **2017**, *110* (19), 193102.

(27) Lee, H. S.; Kim, M. S.; Kim, H.; Lee, Y. H. Identifying multiexcitons in MoS_2 monolayers at room temperature. *Phys. Rev. B: Condens. Matter Mater. Phys.* **2016**, *93* (14), 140409.

(28) Fransted, K. A.; Engel, G. S. Probing vibrational dynamics of PM650 with two-dimensional electronic spectroscopy. *Chem. Phys.* **2012**, *403*, 59−67.

(29) Dahlberg, P. D.; Ting, P.-C.; Massey, S. C.; Allodi, M. A.; Martin, E. C.; Hunter, C. N.; Engel, G. S. Mapping the ultrafast flow of harvested solar energy in living photosynthetic cells. *Nat. Commun.* **2017**, *8* (1), 988.

(30) Allodi, M. A.; Otto, J. P.; Sohail, S. H.; Saer, R. G.; Wood, R. E.; Rolczynski, B. S.; Massey, S. C.; Ting, P.-C.; Blankenship, R. E.; Engel, G. S. Redox Conditions Affect Ultrafast Exciton Transport in Photosynthetic Pigment-Protein Complexes. *J. Phys. Chem. Lett.* **2018**, *9* (1), 89−95.

(31) Caram, J. R.; Zheng, H.; Dahlberg, P. D.; Rolczynski, B. S.; Griffin, G. B.; Fidler, A. F.; Dolzhnikov, D. S.; Talapin, D. V.; Engel, G. S. Persistent Interexcitonic Quantum Coherence in CdSe Quantum Dots. *J. Phys. Chem. Lett.* **2014**, *5* (1), 196−204.

(32) Wang, L.; Williams, N. E.; Malachosky, E. W.; Otto, J. P.; Hayes, D.; Wood, R. E.; Guyot-Sionnest, P.; Engel, G. S. Scalable Ligand-Mediated Transport Synthesis of Organic-Inorganic Hybrid Perovskite Nanocrystals with Resolved Electronic Structure and Ultrafast Dynamics. *ACS Nano* **2017**, *11* (3), 2689−2696.

(33) Kumar, N.; Cui, Q.; Ceballos, F.; He, D.; Wang, Y.; Zhao, H. Exciton-exciton annihilation in $MoSe_2$ monolayers. *Phys. Rev. B: Condens. Matter Mater. Phys.* **2014**, *89* (12), 125427.

(34) Sun, D.; Rao, Y.; Reider, G. A.; Chen, G.; You, Y.; Brézin, L.; Harutyunyan, A. R.; Heinz, T. F. Observation of Rapid Exciton-Exciton Annihilation in Monolayer Molybdenum Disulfide. *Nano Lett.* **2014**, *14* (10), 5625−5629.

(35) Cunningham, P. D.; Hanbicki, A. T.; McCreary, K. M.; Jonker, B. T. Photoinduced Bandgap Renormalization and Exciton Binding Energy Reduction in WS_2. *ACS Nano* **2017**, *11* (12), 12601−12068.

(36) Pogna, E. A.; Marsili, M.; De Fazio, D.; Dal Conte, S.; Manzoni, C.; Sangalli, D.; Yoon, D.; Lombardo, A.; Ferrari, A. C.; Marini, A.; Cerullo, G.; Prezzi, D. Photo-Induced Bandgap Renormalization

Governs the Ultrafast Response of Single-Layer MoS$_2$. *ACS Nano* **2016**, *10* (1), 1182−8.

(37) Sie, E. J.; Frenzel, A. J.; Lee, Y.-H.; Kong, J.; Gedik, N. Intervalley biexcitons and many-body effects in monolayer MoS$_2$. *Phys. Rev. B: Condens. Matter Mater. Phys.* **2015**, *92* (12), 125417.

(38) Aleithan, S. H.; Livshits, M. Y.; Khadka, S.; Rack, J. J.; Kordesch, M. E.; Stinaff, E. Broadband femtosecond transient absorption spectroscopy for a CVD MoS$_2$ monolayer. *Phys. Rev. B: Condens. Matter Mater. Phys.* **2016**, *94* (3), 035445.

(39) Mai, C.; Barrette, A.; Yu, Y.; Semenov, Y. G.; Kim, K. W.; Cao, L.; Gundogdu, K. Many-Body Effects in Valleytronics: Direct Measurement of Valley Lifetimes in Single-Layer MoS$_2$. *Nano Lett.* **2014**, *14* (1), 202−206.

(40) Wang, W.; Sui, N.; Ni, M.; Chi, X.; Pan, L.; Zhang, H.; Kang, Z.; Zhou, Q.; Wang, Y. Studying of the Biexciton Characteristics in Monolayer MoS$_2$. *J. Phys. Chem. C* **2020**, *124* (2), 1749−1754.

(41) Zhao, J.; Zhao, W.; Du, W.; Su, R.; Xiong, Q., Dynamics of exciton energy renormalization in monolayer transition metal disulfides. *Nano Res.* **2020**, DOI: 10.1007/s12274-020-2652-9.

(42) Cho, M. Coherent Two-Dimensional Optical Spectroscopy. *Chem. Rev.* **2008**, *108* (4), 1331−1418.

(43) Brixner, T.; Mančal, T.; Stiopkin, I. V.; Fleming, G. R. Phase-stabilized two-dimensional electronic spectroscopy. *J. Chem. Phys.* **2004**, *121* (9), 4221−4236.

(44) Hybl, J. D.; Albrecht Ferro, A.; Jonas, D. M. Two-dimensional Fourier transform electronic spectroscopy. *J. Chem. Phys.* **2001**, *115* (14), 6606−6622.

(45) Masumoto, Y.; Fluegel, B.; Meissner, K.; Koch, S. W.; Binder, R.; Paul, A.; Peyghambarian, N. Band-gap renormalization and optical gain formation in highly excited CdSe. *J. Cryst. Growth* **1992**, *117* (1), 732−737.

(46) Liu, F.; Ziffer, M. E.; Hansen, K. R.; Wang, J.; Zhu, X. Direct Determination of Band-Gap Renormalization in the Photoexcited Monolayer MoS$_2$. *Phys. Rev. Lett.* **2019**, *122* (24), 246803.

(47) Guo, L.; Wu, M.; Cao, T.; Monahan, D. M.; Lee, Y.-H.; Louie, S. G.; Fleming, G. R. Exchange-driven intravalley mixing of excitons in monolayer transition metal dichalcogenides. *Nat. Phys.* **2019**, *15* (3), 228−232.

(48) Zheng, H.; Caram, J. R.; Dahlberg, P. D.; Rolczynski, B. S.; Viswanathan, S.; Dolzhnikov, D. S.; Khadivi, A.; Talapin, D. V.; Engel, G. S. Dispersion-free continuum two-dimensional electronic spectrometer. *Appl. Opt.* **2014**, *53* (9), 1909−1917.

(49) Singh, V. P.; Fidler, A. F.; Rolczynski, B. S.; Engel, G. S. Independent phasing of rephasing and non-rephasing 2D electronic spectra. *J. Chem. Phys.* **2013**, *139* (8), 084201.

(50) You, Y.; Zhang, X.-X.; Berkelbach, T. C.; Hybertsen, M. S.; Reichman, D. R.; Heinz, T. F. Observation of biexcitons in monolayer WSe$_2$. *Nat. Phys.* **2015**, *11* (6), 477−481.

(51) Hao, K.; Specht, J. F.; Nagler, P.; Xu, L.; Tran, K.; Singh, A.; Dass, C. K.; Schüller, C.; Korn, T.; Richter, M.; Knorr, A.; Li, X.; Moody, G. Neutral and charged inter-valley biexcitons in monolayer MoSe$_2$. *Nat. Commun.* **2017**, *8* (1), 15552.

(52) Trankle, G.; Lach, E.; Forchel, A.; Scholz, F.; Ell, C.; Haug, H.; Weimann, G.; Griffiths, G.; Kroemer, H.; Subbanna, S. General relation between band-gap renormalization and carrier density in two-dimensional electron-hole plasmas. *Phys. Rev. B: Condens. Matter Mater. Phys.* **1987**, *36* (12), 6712−6714.

(53) Sie, E. J.; Steinhoff, A.; Gies, C.; Lui, C. H.; Ma, Q.; Rosner, M.; Schonhoff, G.; Jahnke, F.; Wehling, T. O.; Lee, Y. H.; Kong, J.; Jarillo-Herrero, P.; Gedik, N. Observation of Exciton Redshift-Blueshift Crossover in Monolayer WS$_2$. *Nano Lett.* **2017**, *17* (7), 4210−4216.

(54) Berghäuser, G.; Bernal-Villamil, I.; Schmidt, R.; Schneider, R.; Niehues, I.; Erhart, P.; Michaelis de Vasconcellos, S.; Bratschitsch, R.; Knorr, A.; Malic, E. Inverted valley polarization in optically excited transition metal dichalcogenides. *Nat. Commun.* **2018**, *9* (1), 971.

(55) Selig, M.; Katsch, F.; Schmidt, R.; Michaelis de Vasconcellos, S.; Bratschitsch, R.; Malic, E.; Knorr, A. Ultrafast dynamics in monolayer transition metal dichalcogenides: Interplay of dark excitons, phonons, and intervalley exchange. *Phys. Rev. Research* **2019**, *1* (2), 022007.

(56) Wang, Z.; Molina-Sánchez, A.; Altmann, P.; Sangalli, D.; De Fazio, D.; Soavi, G.; Sassi, U.; Bottegoni, F.; Ciccacci, F.; Finazzi, M.; Wirtz, L.; Ferrari, A. C.; Marini, A.; Cerullo, G.; Dal Conte, S. Intravalley Spin-Flip Relaxation Dynamics in Single-Layer WS$_2$. *Nano Lett.* **2018**, *18* (11), 6882−6891.

(57) Wang, L.; Wu, M. W. Electron spin relaxation due to D'yakonov-Perel' and Elliot-Yafet mechanisms in monolayer MoS$_2$: Role of intravalley and intervalley processes. *Phys. Rev. B: Condens. Matter Mater. Phys.* **2014**, *89* (11), 115302.

(58) Wang, L.; Wu, M. W. Intrinsic electron spin relaxation due to the D'yakonov-Perel' mechanism in monolayer MoS2. *Phys. Lett. A* **2014**, *378* (18), 1336−1340.

(59) Manca, M.; Glazov, M. M.; Robert, C.; Cadiz, F.; Taniguchi, T.; Watanabe, K.; Courtade, E.; Amand, T.; Renucci, P.; Marie, X.; Wang, G.; Urbaszek, B. Enabling valley selective exciton scattering in monolayer WSe$_2$ through upconversion. *Nat. Commun.* **2017**, *8* (1), 14927.

(60) Bernal-Villamil, I.; Berghäuser, G.; Selig, M.; Niehues, I.; Schmidt, R.; Schneider, R.; Tonndorf, P.; Erhart, P.; de Vasconcellos, S. M.; Bratschitsch, R.; Knorr, A.; Malic, E. Exciton broadening and band renormalization due to Dexter-like intervalley coupling. *2D Mater.* **2018**, *5* (2), 025011.

(61) Zhang, C.; Wang, H.; Chan, W.; Manolatou, C.; Rana, F., Absorption of Light by Excitons and Trions in Monolayers of Metal Dichalcogenide MoS$_2$: Experiments and Theory. *Phys. Rev. B: Condens. Matter Mater. Phys.* **2014**, *89*, DOI: 10.1103/PhysRevB.89.205436.

(62) Moody, G.; Kavir Dass, C.; Hao, K.; Chen, C.-H.; Li, L.-J.; Singh, A.; Tran, K.; Clark, G.; Xu, X.; Berghäuser, G.; Malic, E.; Knorr, A.; Li, X. Intrinsic homogeneous linewidth and broadening mechanisms of excitons in monolayer transition metal dichalcogenides. *Nat. Commun.* **2015**, *6* (1), 8315.

(63) Sim, S.; Park, J.; Song, J.-G.; In, C.; Lee, Y.-S.; Kim, H.; Choi, H. Exciton dynamics in atomically thin MoS$_2$: Interexcitonic interaction and broadening kinetics. *Phys. Rev. B: Condens. Matter Mater. Phys.* **2013**, *88* (7), 075434.

(64) Richter, J. M.; Branchi, F.; Valduga de Almeida Camargo, F.; Zhao, B.; Friend, R. H.; Cerullo, G.; Deschler, F. Ultrafast carrier thermalization in lead iodide perovskite probed with two-dimensional electronic spectroscopy. *Nat. Commun.* **2017**, *8* (1), 376.

(65) Ruppert, C.; Chernikov, A.; Hill, H. M.; Rigosi, A. F.; Heinz, T. F. The Role of Electronic and Phononic Excitation in the Optical Response of Monolayer WS$_2$ after Ultrafast Excitation. *Nano Lett.* **2017**, *17* (2), 644−651.

(66) Czech, K. J.; Thompson, B. J.; Kain, S.; Ding, Q.; Shearer, M. J.; Hamers, R. J.; Jin, S.; Wright, J. C. Measurement of Ultrafast Excitonic Dynamics of Few-Layer MoS2 Using State-Selective Coherent Multidimensional Spectroscopy. *ACS Nano* **2015**, *9* (12), 12146−12157.

(67) Turner, D. B.; Wen, P.; Arias, D. H.; Nelson, K. A.; Li, H.; Moody, G.; Siemens, M. E.; Cundiff, S. T. Persistent exciton-type many-body interactions in GaAs quantum wells measured using two-dimensional optical spectroscopy. *Phys. Rev. B: Condens. Matter Mater. Phys.* **2012**, *85* (20), 201303.

(68) Borca, C. N.; Zhang, T.; Li, X.; Cundiff, S. T. Optical two-dimensional Fourier transform spectroscopy of semiconductors. *Chem. Phys. Lett.* **2005**, *416* (4), 311−315.

(69) Nardin, G.; Moody, G.; Singh, R.; Autry, T. M.; Li, H.; Morier-Genoud, F.; Cundiff, S. T. Coherent Excitonic Coupling in an Asymmetric Double InGaAs Quantum Well Arises from Many-Body Effects. *Phys. Rev. Lett.* **2014**, *112* (4), 046402.

(70) Zhang, T.; Kuznetsova, I.; Meier, T.; Li, X.; Mirin, R. P.; Thomas, P.; Cundiff, S. T. Polarization-dependent optical 2D Fourier transform spectroscopy of semiconductors. *Proc. Natl. Acad. Sci. U. S. A.* **2007**, *104* (36), 14227.

(71) Bristow, A. D.; Karaiskaj, D.; Dai, X.; Mirin, R. P.; Cundiff, S. T. Polarization dependence of semiconductor exciton and biexciton

contributions to phase-resolved optical two-dimensional Fourier-transform spectra. *Phys. Rev. B: Condens. Matter Mater. Phys.* **2009**, *79* (16), 161305.

(72) Smallwood, C. L.; Cundiff, S. T. Multidimensional Coherent Spectroscopy of Semiconductors. *Laser Photonics Rev.* **2018**, *12* (12), 1800171.

(73) Li, H.; Cundiff, S. T., Chapter One - 2D Coherent Spectroscopy of Electronic Transitions. In *Advances in Atomic, Molecular, and Optical Physics*; Arimondo, E.; Lin, C. C.; Yelin, S. F., Eds.; Academic Press: 2017; Vol. *66*, pp 1−48.

(74) Chemla, D. S.; Shah, J. Many-body and correlation effects in semiconductors. *Nature* **2001**, *411* (6837), 549−557.

(75) Singh, R.; Moody, G.; Siemens, M. E.; Li, H.; Cundiff, S. T. Quantifying spectral diffusion by the direct measurement of the correlation function for excitons in semiconductor quantum wells. *J. Opt. Soc. Am. B* **2016**, *33* (7), C137.

(76) Šanda, F.; Perlík, V.; Lincoln, C. N.; Hauer, J. Center Line Slope Analysis in Two-Dimensional Electronic Spectroscopy. *J. Phys. Chem. A* **2015**, *119* (44), 10893−10909.

(77) Lietard, A.; Hsieh, C.-S.; Rhee, H.; Cho, M. Electron heating and thermal relaxation of gold nanorods revealed by two-dimensional electronic spectroscopy. *Nat. Commun.* **2018**, *9*, 891.

(78) Kwak, K.; Park, S.; Finkelstein, I. J.; Fayer, M. D. Frequency-frequency correlation functions and apodization in two-dimensional infrared vibrational echo spectroscopy: A new approach. *J. Chem. Phys.* **2007**, *127* (12), 124503.

(79) Fenn, E. E.; Fayer, M. D. Extracting 2D IR frequency-frequency correlation functions from two component systems. *J. Chem. Phys.* **2011**, *135* (7), 074502.

(80) Kim, M. S.; Yun, S. J.; Lee, Y.; Seo, C.; Han, G. H.; Kim, K. K.; Lee, Y. H.; Kim, J. Biexciton Emission from Edges and Grain Boundaries of Triangular WS_2 Monolayers. *ACS Nano* **2016**, *10* (2), 2399−2405.

(81) Barbone, M.; Montblanch, A. R. P.; Kara, D. M.; Palacios-Berraquero, C.; Cadore, A. R.; De Fazio, D.; Pingault, B.; Mostaani, E.; Li, H.; Chen, B.; Watanabe, K.; Taniguchi, T.; Tongay, S.; Wang, G.; Ferrari, A. C.; Atatüre, M. Charge-tuneable biexciton complexes in monolayer WSe_2. *Nat. Commun.* **2018**, *9* (1), 3721.

(82) Li, Z.; Wang, T.; Lu, Z.; Jin, C.; Chen, Y.; Meng, Y.; Lian, Z.; Taniguchi, T.; Watanabe, K.; Zhang, S.; Smirnov, D.; Shi, S.-F. Revealing the biexciton and trion-exciton complexes in BN encapsulated WSe_2. *Nat. Commun.* **2018**, *9* (1), 3719.

(83) Schmitt-Rink, S.; Ell, C.; Koch, S. W.; Schmidt, H. E.; Haug, H. Subband-level renormalization and absorptive optical bistability in semiconductor multiple quantum well structures. *Solid State Commun.* **1984**, *52* (2), 123−125.

(84) Trovatello, C.; Miranda, H. P. C.; Molina-Sánchez, A.; Varillas, R. B.; Moretti, L.; Ganzer, L.; Maiuri, M.; Soavi, G.; Ferrari, A. C.; Marini, A.; Wirtz, L.; Cerullo, G.; Sangalli, D.; Conte, S. D. Strong Exciton-Coherent Phonon Coupling in Single-Layer MoS_2. *Conference on Lasers and Electro-Optics*; Optical Society of America: San Jose, CA, 2019; p FW3M.7.

(85) Carvalho, B. R.; Malard, L. M.; Alves, J. M.; Fantini, C.; Pimenta, M. A. Symmetry-Dependent Exciton-Phonon Coupling in 2D and Bulk MoS_2 Observed by Resonance Raman Scattering. *Phys. Rev. Lett.* **2015**, *114* (13), 136403.

(86) Arora, A.; Nogajewski, K.; Molas, M.; Koperski, M.; Potemski, M. Exciton band structure in layered $MoSe_2$: from a monolayer to the bulk limit. *Nanoscale* **2015**, *7* (48), 20769−20775.

(87) Molas, M. R.; Faugeras, C.; Slobodeniuk, A. O.; Nogajewski, K.; Bartos, M.; Basko, D. M.; Potemski, M. Brightening of dark excitons in monolayers of semiconducting transition metal dichalcogenides. *2D Mater.* **2017**, *4* (2), 021003.

(88) Dahlberg, P. D.; Fidler, A. F.; Caram, J. R.; Long, P. D.; Engel, G. S. Energy Transfer Observed in Live Cells Using Two-Dimensional Electronic Spectroscopy. *J. Phys. Chem. Lett.* **2013**, *4* (21), 3636−3640.